

# Improving the Performance of Chaos-Based Modulations Via Serial Concatenation

Francisco J. Escribano, *Member, IEEE*, Luis López, and Miguel A. F. Sanjuán

**Abstract**—This paper proposes a serially concatenated system with an outer convolutional channel encoder and an inner chaos-based coded modulator. With the help of the principles of symbolic dynamics, the chaotic modulation can be described in terms of a trellis. Owing to this, we show that the resulting system can be designed and analyzed following developments made for serially concatenated channel codes (SCCCs) or bit-interleaved coded-modulation systems. We show how the iterative decoding algorithm used in this concatenated framework can be analyzed through the well-known extrinsic information transfer chart device and how the bit error rate can be bounded using the transfer function of the convolutional channel encoder. Comparison with a related SCCC system in both additive white Gaussian noise and frequency-nonsselective fading channels shows that this kind of chaos-based systems keeps the potential advantages of coded-modulation-based systems. We are thus confident that the principles shown here can lead to the design of competitive chaotic discrete communication systems.

**Index Terms**—Channel coding, chaos, concatenated coding, fading channels, modulation coding.

## I. INTRODUCTION

THE possibility of using chaotic signals to carry information was first considered in 1993 [1]. This aroused a big deal of work on chaotic communications, which became a hot topic in both nonlinear science and engineering. The interest in chaotic communications was due to the foreseen good properties of the chaotic signals in the fields of secure systems or broadband multiple-access systems. In the case of secure systems, one could take advantage of the uncorrelation and unpredictability of the chaotic signals to build encryption algorithms. These are the same properties desirable for the spread sequences of a code-division multiple-access system. On the other hand, chaotic modulations and channel encoders derived from chaotic systems attracted much attention, but the interest on this kind

of chaotic communications dropped somewhat due to the bad performance of the systems proposed so far. In fact, they did not outperform other usual coded communication schemes, and they did not have even better performance than uncoded systems [2]–[5].

However, in later times and in some contexts, we have witnessed the arising of some proposals with good performances as compared with classical communication systems [6]. Some recent proposals make use of the fact that chaos-based systems can be good for secure communications [7], [8]. This has reopened the trend of looking for efficient chaotic systems included in classical schemes where the potentiality of chaos in the channel could be properly exploited. Some chaos-based modulation systems working at the waveform level have already shown to be of potential use in multipath fading channels [9]. Other kinds of chaos-based systems working at the coding level [10]–[12] have shown to provide good results in multiuser channels. Other recent works have stressed the fact that chaos-based coded modulated systems working at a joint waveform and coding level can be efficient in additive white Gaussian noise (AWGN) [6], [13], [14]. It has been also shown that communications based on highly dimensional chaotic systems and belief propagation decoding can offer an excellent performance characterized with thresholds [15]. Moreover, chaos-based coded-modulation systems have proved to be of potential interest in flat fading channels [16] or under intersymbol interference [17]. This relative success, which contrasts strongly with previous state of the art, has been achieved by building a comprehensive bridge linking the fields of chaos theory and digital communications.

In particular, the proposal of a kind of chaos-based coded modulations which could be seen under a trellis encoding view [6] opened the road to evaluate such kind of encoders in the same schemes where convolutional codes (CCs) or trellis-coded-modulation (TCM) systems are able to yield high coding gains. For example, it is already possible to build very efficient coded and modulated systems using concatenation: parallel concatenation, such as that in the so-called turbocodes or turbo TCM (TTCM) systems [18], or serial concatenation, such as that in serially concatenated CCs (SCCCs), serially concatenated TCM (SCTCM) systems [18], or bit-interleaved coded modulations (BICMs) [19].

The convolutional encoder view of the mentioned kind of chaos-based coded modulations is much like Ungerboeck's TCM [18], and since the TTCM systems combining the bandwidth-efficient TCM systems and the philosophy of turbocoding offer good performance in white noise and radio channels, it was expected that new systems built under the same principles could lead to comparable results. This has been ascertained in [13], where parallel concatenated chaos-based

Manuscript received November 06, 2008; revised January 27, 2009. First published March 27, 2009; current version published February 10, 2010. This work was supported in part by the by the Spanish Ministry of Education and Science under Project FIS2006-08525, by the Spanish Ministry of Science and Innovation under Project FIS2009-09898 and Project PET2008-0128, by the Spanish Ministry of Industry under Project TSI-020110-2009-103, and by Comunidad de Madrid under Project S2009TIC-1692 (CLOUDS). This paper was recommended by Associate Editor Z. Galias.

F. J. Escribano is with the Departamento de Teoría de la Señal y Comunicaciones, Escuela Politécnica Superior, Universidad de Alcalá de Henares, 28805 Alcalá de Henares, Spain (e-mail: francisco.escribano@ieeee.org).

L. López is with the Departamento de Sistemas Telemáticos y Computación, Universidad Rey Juan Carlos, 28933 Móstoles, Spain (e-mail: luis.lopez@urjc.es).

M. A. F. Sanjuán is with the Departamento de Física, Universidad Rey Juan Carlos, 28933 Móstoles, Spain (e-mail: miguel.sanjuán@urjc.es).

Digital Object Identifier 10.1109/TCSI.2009.2019408

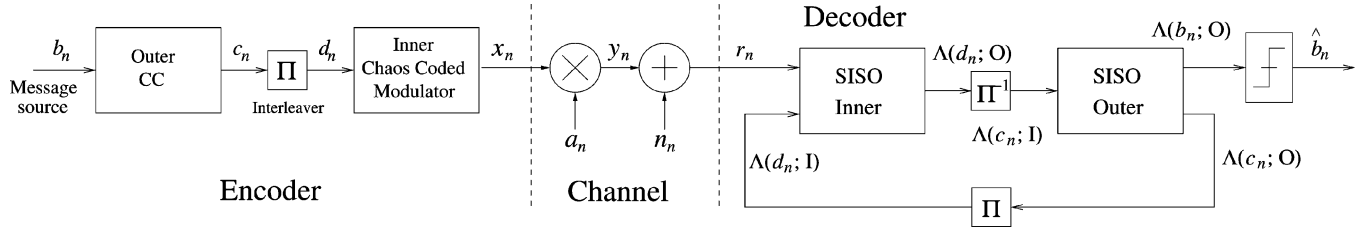


Fig. 1. Block diagram of the concatenated encoder, the distorting channel, and the iterative decoder.

coded modulations have shown to give coding gains as high as with standard binary turbocodes. Another advantage of designing systems under these similarities is that we can use well-established tools to design the encoders and decoders and to evaluate their performance, thus avoiding the need to start from scratch or just relying on complex chaos theory. The use of the extrinsic information transfer (EXIT) charts to evaluate the convergence of the decoding algorithm in [13] is an instance of this.

Other examples of the success of this philosophy in chaotic communications is the proposal of [20], where the trellis encoder view allowed the design of systems with serially concatenated channel and chaotic encoders, leading to potentially good bit-error-rate (BER) results. However, the developments of [20] lacked of a comprehensive study and sufficient theoretical grounds that are fully developed here. Moreover, since systems based on TCM are supposed to behave well in fading channels (namely, SCTCM and BICM) [21], we extend the study of our chaotic communications systems to frequency-nonselective Rician fading channels.

According to these aims, this paper is structured as follows. In Section II, we will describe in detail the whole communications system, including the concatenated encoder, the channel, and the iterative decoder. Section III will show how the behavior of this chaos-based serially concatenated system can be understood from chaos theory principles. In Section IV, we will show how to analyze the iterative decoder with the help of the EXIT chart tool. Section V is devoted to the calculation of bit error probability bounds. Section VI will show the simulation results and the validation of the previous analysis. Finally, Section VII is devoted to the conclusions.

## II. SYSTEM MODEL

### A. Concatenated Encoder

As stated, this paper deals with a serially concatenated system with interleavers, where we make use of chaos-based coded modulations instead of standard channel encoders or TCM systems. According to this, we will call this system serially concatenated chaos-coded modulation (SCCCM), whose corresponding scheme can be seen in Fig. 1. We have, as outer encoder, a CC of rate  $R_{CC}$ , which accepts as input an independent and identically distributed (i.i.d.) binary sequence  $b_n$  and produces a convolutionally coded binary sequence  $c_n$ . This outer CC can be either recursive or nonrecursive [22]. As the interleaver works with input bit blocks of size  $N$  to produce the scrambled sequence  $d_n$  and as we perform trellis termination in the CC, each input block for the inner encoder will be produced by a message sequence of size  $k = R_{CC} \cdot N - \nu$ , where  $\nu = m + 1$  is the constraint length of the CC and  $m$  is

its memory length. The interleaver considered here will be an S-Random interleaver [18], where the permutation function is chosen in a semirandom basis. This function will map an index  $j$  into an index  $\pi_j$ , so that the bit in position  $j$ , i.e.,  $c_j$ , at the output of the outer encoder will be taken as a bit in position  $\pi_j$ , i.e.,  $d_{\pi_j}$ , at the input of the inner encoder. The index permutation is chosen according to the following algorithm.

- 1) Choose an integer  $S$ .
- 2) For index  $\pi_j$  corresponding to position  $j$ , draw a random number  $t$  between 1 and  $N$ .
- 3) If  $t$  has not been chosen before, verify if the  $S$  previously chosen indexes lie at least at a distance of  $S$  from  $t$ , i.e.,  $|\pi_p - t| > S$  for  $p = j - S, \dots, j - 1$ .
- 4) If  $t$  satisfies the conditions, keep it as  $\pi_j = t$  and proceed until all  $N$  indexes are chosen.

This algorithm converges in a reasonable time when  $S$  is chosen according to

$$S < \sqrt{\frac{N}{2}}. \quad (1)$$

When  $S = 1$ , we have a purely random interleaver. Taking  $S$  with higher values ensures us that the adjacent bits in the CC output word  $\mathbf{c} = (c_1, \dots, c_N)$  will be at least separated in  $S$  positions within the input word  $\mathbf{d} = (d_1, \dots, d_N)$  for the inner encoder [18].

The inner encoder is a chaos-based coded modulator driven by small perturbations [6], where the output is recursively given by

$$z_n = f(z_{n-1}) + g(d_{n-1}, z_{n-1}) \cdot 2^{-Q} \quad (2)$$

$$x_n = 2z_n - 1 \quad (3)$$

where  $f(z) : [0, 1] \rightarrow [0, 1]$  is a chaotic map and  $g(d, z) \in \{0, 1\}$  is a binary function whose meaning will be explained in the sequel. Note that  $x_n \in [-1, 1]$  and that the rate of the chaos-based coded modulation is one symbol per bit. In our developments, we will make use of the Bernoulli shift map (BSM), which is  $f(z) = 2z \bmod 1$ , since this is the simplest case and can thus help to understand the behavior of the whole system. It is easy to show that a recursion like (2) leaves the finite set  $S_Q = \{m \cdot 2^{-Q} | m = 0, \dots, 2^Q - 1\}$  invariant, and therefore, we can restrict (2) to  $S_Q$  by taking as initial condition  $z_0$  any point in  $S_Q$  (e.g.,  $z_0 = 0$ ) [6]. When  $Q \rightarrow \infty$ , (2) becomes simply the recursion by the chaotic map  $f(z)$  without control. It is a general principle in concatenated coding that the inner encoder has to be recursive in order to get interleaver gain [18], and this is the reason to define  $g(d, z)$  as

$$g(d, z) = \begin{cases} d, & z < \frac{1}{2} \\ \bar{d}, & z \geq \frac{1}{2} \end{cases} \quad (4)$$

where  $\bar{d} = d \otimes 1$  and  $\otimes$  is the binary XOR operation. All this becomes clearer if we look into the trellis encoder view of this chaos-based coded modulator [6], which can be developed through the associated symbolic dynamics [23]. In fact, when  $z_0 = 0$ , the encoder based upon the BSM can be seen as a shift register with  $Q$  memory positions storing  $Q$  successive values of  $g(d_n, z_n)$  and where the output  $z_n$  is calculated as

$$z_n = \sum_{m=1}^Q g(d_{n-m}, z_{n-m}) \cdot 2^{m-Q-1} \quad (5)$$

where  $g(d_n, z_n) = d_n \otimes d_{n-Q+1}$ , which is equivalent to (4). Although, in this paper, we focus only on the simple case of the BSM for illustrative purposes, there is a whole kind of chaos-based coded modulators based upon the same principles that could be employed in this same framework and that could be described by an equivalent trellis encoder [6]. Note also that, since  $g(d, z)$  is equivalent to a precoder of the kind  $1 + D^Q$ , it will always be possible to include such kind of simple recursive precoder (rate 1 accumulate code) before the chaos-based coded modulator, as is usually done in turbo equalization [24] or in SCTCM systems [25] in order to preserve the interleaver gain. In the context of chaos-based coded modulations used within serial concatenated schemes, the key role of feedback on the inner encoder can be verified by comparing the results of [20] with the present results. Although the principles of the SCCCM systems were first examined there [20], this paper greatly expands those primary results and builds a comprehensive framework for the further development of useful SCCCM systems.

Once modulated, the samples  $x_n$  are sent to the channel in baseband. Although each  $x_n$  conveys information about  $Q$  bits, we do not puncture the sequence  $x_n$  produced by relations (2) and (3). As the encoder thus defined produces one  $x_n$  sample per input bit  $d_n$ , the rate of the chaos-based coded modulation is 1 sample/bit. Therefore, the overall rate of the concatenated system is  $R = R_{CC}$ . This is a main difference with respect to SCTCM, since we do not look for spectral efficiency, and this is the reason why these SCCCM systems have to be compared mainly with SCC systems.

### B. Channel

In the channel (see Fig. 1),  $x_n$  can be subjected to the effects of only AWGN or AWGN plus frequency-nonspecific Rician flat fading. Therefore, the sequence  $\mathbf{r} = (r_1, \dots, r_N)$  arriving at the decoder side can be, in general, described by

$$r_n = y_n + n_n = a_n x_n + n_n \quad (6)$$

where  $n_n$  is a sequence of the i.i.d. samples of a Gaussian process with zero mean and power  $\sigma^2$  and  $a_n$  is a sequence of the uncorrelated samples of a Rician process. The samples  $a_n$  follow the probability density function (pdf)

$$p(a) = 2a(1+K)e^{-a^2(1+K)-K} I_0\left(2a\sqrt{K(K+1)}\right), \quad a \geq 0 \quad (7)$$

where  $I_0(\cdot)$  is the zeroth-order modified Bessel function of the first kind and  $K$  is the ratio of specular to diffuse energy [21].  $K = 0$  corresponds to the Rayleigh channel case, and  $K \rightarrow \infty$  corresponds to the pure AWGN channel. For the channel only

affected by AWGN, we set  $a_n = 1$ . The mean and variance of the Rician process are given by

$$\eta_a = \frac{1}{2} \sqrt{\frac{\pi}{1+K}} e^{-\frac{K}{2}} \left[ (1+K) I_0\left(\frac{K}{2}\right) + K I_1\left(\frac{K}{2}\right) \right] \\ \sigma_a^2 = 1 - \eta_a^2 \quad (8)$$

where  $I_1(\cdot)$  is the first-order modified Bessel function of the first kind. Note that  $E[a^2] = 1$ , so that the signal-to-noise ratios at the transmitter and decoder sides are the same. The noise power is related to the signal-to-noise ratio as  $\sigma^{-2} = 2(R/P)(E_b/N_0)$ , where  $P = 1/3$  is the power of the chaos-based coded modulated signal  $x_n$  for the BSM encoder, since  $P = 1/12$  for  $z_n$  [6]. This value of  $P$  corresponds to the case when  $Q \rightarrow \infty$ , but the difference with respect to the real value when  $Q \geq 4$  is negligible for our purposes [4].

### C. Iterative Decoder

According to the serially concatenated nature of the encoded data, each block of  $N$  samples  $\mathbf{r} = (r_1, \dots, r_N)$  is finally decoded by means of an iterative decoder, as shown in Fig. 1. This iterative decoder is based upon two soft-input–soft-output (SISO) modules [18] linked by means of a corresponding interleaver  $\Pi$  and a corresponding deinterleaver  $\Pi^{-1}$ . The SISO module for the chaos-based coded modulation is based on an adaptation of the usual SISO block implementing the *maximum a posteriori* (MAP) Bahl–Cocke–Jelinek–Raviv (BCJR) backward–forward algorithm [26]. It takes advantage of the trellis encoding equivalence of the chaotic modulation and its underlying symbolic dynamics, as shown in [20]. Since we do not perform any trellis termination in the inner encoder, the ending state of the data block for the inner SISO will be unknown, and the backward calculation of the MAP algorithm will be performed by initializing the values equiprobably [18]. It is possible to think of getting some enhancement by using trellis termination in the inner chaos-based coded modulator, but a good design of the interleaver and a high value of the block length  $N$  has been shown to be enough to make the difference between trellis termination and non trellis termination negligible [27].

In case of perfect channel state information (CSI), the inner SISO module provides the extrinsic information in the form of log probability estimations

$$\Lambda(d_n; \mathbf{O}) = \log \left( \frac{P(d_n = 1 | \mathbf{r}, \mathbf{a})}{P(d_n = 0 | \mathbf{r}, \mathbf{a})} \right) \quad (9)$$

where  $\mathbf{a} = (a_1, \dots, a_N)$  is the vector of fading amplitudes. When no CSI is available, the output of the SISO is calculated as

$$\Lambda(d_n; \mathbf{O}) = \log \left( \frac{P(d_n = 1 | \mathbf{r}, \eta_a)}{P(d_n = 0 | \mathbf{r}, \eta_a)} \right). \quad (10)$$

When we are in the pure AWGN channel, the log probability estimations take the form

$$\Lambda(d_n; \mathbf{O}) = \log \left( \frac{P(d_n = 1 | \mathbf{r})}{P(d_n = 0 | \mathbf{r})} \right). \quad (11)$$

The parameters  $\mathbf{O}$  and  $\mathbf{I}$  in the log probabilities of Fig. 1 stand for output and input, respectively. The metrics for the MAP

algorithm within the inner SISO module will be calculated as  $|r_n - x^*|$  for the AWGN case, as  $|r_n - a_n x^*|$  in the fading channel with CSI, and as  $|r_n - \eta_a x^*|$  for the fading channel without CSI [28].  $x^* = 2z^* - 1$ , where  $z^* \in S_Q$ , is the quantized value for the chaotic sample taken as candidate to calculate the metric with respect to the received sample  $r_n$  [26]. This means that, for each sample  $r_n$  from the channel, there are  $2^Q$  potential metrics to be calculated. After several decoding iterations through the inner and outer SISO modules, we get an estimated decoded sequence  $\hat{b}_n$ .

### III. ENCODING WITH INITIAL CONDITIONS: A CHAOS THEORY POINT OF VIEW

The chaos-based coded modulation employed is an instance of a controlled 1-D modulation using an underlying chaotic map [6], which, in the case of the BSM, consists of an adaptation of the principle of *encoding with initial conditions* to avoid the need for infinite precision [4], [29]. In the ideal case, when  $Q \rightarrow \infty$ , (2) tends to the uncontrolled case where the chaotic samples are produced following the exact dynamics of the chaotic map

$$z_n = f(z_{n-1}). \quad (12)$$

We can apply symbolic dynamics and consider the bit sequence produced by assigning the bit 0 to the samples confined to the  $[0, 1/2)$  interval and the bit 1 to the samples belonging to the  $[1/2, 1]$  interval, i.e.,

$$b_n = \left\lfloor x_n + \frac{1}{2} \right\rfloor. \quad (13)$$

In this case, it is easy to show that the initial condition  $z_0$  has an associated binary expansion exactly corresponding to such bit sequence

$$z_0 = \sum_{n=1}^{\infty} b_n \cdot 2^{-n}. \quad (14)$$

The ideal system with  $Q \rightarrow \infty$  cannot be used in practice, since we would require the definition of  $z_0$  with infinite precision. This is the reason to propose the quantized and controlled version. Nevertheless, the limit with  $Q \rightarrow \infty$  has been usefully employed in examining the Euclidean distance properties of some chaos-based coded modulations, like the ones employing the BSM and the tent map [30]. These results have been shown to be largely valid in the feasible chaos-based coded modulated version with  $Q < \infty$ . On the other hand, it has been shown that, in the case of the BSM system, the minimum Euclidean distance between possible unconstrained sequences produced by iterating through the map corresponds to the case of sequences generated by ideal initial conditions  $z_0$  and  $z'_0$  differing in only 1 bit

$$d_{E_{\min}}^2 = d^2(\{z_n\}, \{z'_n\}) = \sum_{n=0}^{\infty} (z_n - z'_n)^2 = \frac{1}{3} \quad (15)$$

which makes a system based on BSM no better than uncoded binary-phase shift keying (BPSK) [30]. The minimum Euclidean distance for the feasible case with  $Q < \infty$  tends rapidly to the theoretical value even for low values of  $Q$ . One way of overcoming the general poor distance properties of the rate 1 coded

modulations thus produced has been increasing the dimensionality of the dynamical systems involved while providing a new general framework for chaos-based coded modulations [6].

Another possible way to increase Euclidean distance in related chaos-based modulation systems is the definition of fractal sets for the initial conditions [31]. In this case, the ideal initial condition  $z_0$  could not be chosen outside a fractal subset contained in  $[0, 1]$ . Owing to this, the minimum Euclidean distance is no longer related to initial conditions differing in only 1 bit in their respective binary expansions. The problem is that this device does not prevent the possibility of catastrophic decoding, i.e., the possibility of choosing in error a sequence of chaotic samples at a finite Euclidean distance of the original one, but leading to a virtually infinite number of decoding bit errors [31].

If we look into the structure of our complete serially concatenated system, we can see that, in the ideal case where  $N \rightarrow \infty$  and  $Q \rightarrow \infty$ , the possible ideal initial conditions for the BSM  $z_0 = \sum_{n=1}^{\infty} 2^{-n} d_n$  cannot take arbitrary values due to the interleaving and to the convolutional coding. If  $d_{\text{free}}$  is the free distance of the outer CC, the codeword sequences  $c_n$  will differ at least in  $d_{\text{free}}$  bits. This is basically the same principle followed in the design of fractal sets.

However, the benefit of concatenation not only lies in the final increase in minimum Euclidean distance for the equivalent chaos-based coded modulated system. It also provides an intrinsically noncatastrophic decoder. The iterative decoder based on SISO probabilistic estimations has shown to be robust and well behaving once convergence threshold is reached [18]. We will see this clearly in the examples of Section VI. Therefore, we can rely on known developments within communications theory and apply them in the design and evaluation of this kind of concatenated chaotic systems. In the following two sections, we will exploit these analogies and show how we can study the convergence threshold of the iterative decoding algorithm and how we can get bounds for the bit error probability. All this will help in strengthening the useful links between standard communications theory and chaos-based communications.

### IV. CONVERGENCE ANALYSIS

In this section, we study the behavior of the iterative decoding algorithm for the proposed channels. A powerful tool to look into the convergence of this algorithm as a function of channel distortion is the so-called EXIT charts [32]. They have proved to be useful as design tools not only in the context of binary turbocodes or in serial concatenation of binary codes but also with TCM systems [33] and in the evaluation of turbo-equalized systems [34]. The EXIT charts are based upon the computation of the mutual information of the log probability estimations at the input of the SISO module versus the mutual information of the log probability estimations at the output of the SISO module after a decoding step. This mutual information  $I$  is calculated as [18]

$$I = \frac{1}{2} \sum_{d=0,1}^{\infty} \int_{-\infty}^{\infty} p(\Lambda|d) \log_2 \left( \frac{2p(\Lambda|d)}{p(\Lambda|1) + p(\Lambda|0)} \right) d\Lambda \quad (16)$$

where  $p(\Lambda|d)$  is the pdf of the log probability estimation when the bit sent takes the value  $d$ . We have dropped the index in  $d$  for simplicity. In Fig. 2, we can see a scheme of the setup for

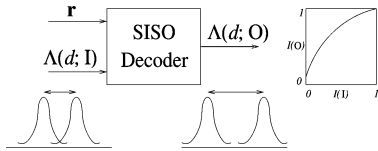


Fig. 2. Decoding behavior of the SISO module.

the inner decoder where we have shown the distribution of a set of input log probability estimations ( $\Lambda(d; I)$ ) with two peaks corresponding to each case, i.e.,  $d = 0$  and  $d = 1$ . If the decoding algorithm is working well for the level of distortion in the channel, the distribution of the output log probability estimations ( $\Lambda(d; O)$ ) will have the two peaks more distinctly separated, which means a higher probability to decode without error and also a growing value of the mutual information  $I$ , as shown in the related  $I(O)/I(I)$  curve (O: output; I: input).

Although Fig. 2 refers to the SISO module for the chaos-based coded modulation, the same principles are straightforwardly applicable to the SISO module for the CC, just by renaming the input and output as in Fig. 1, so that the input and output mutual information will be calculated over  $\Lambda(c; I)$  and  $\Lambda(c; O)$ , respectively. Note that the  $I(O)/I(I)$  curve depends on the channel distortion level for the inner SISO module (it makes use of the channel output  $\mathbf{r}$  to calculate  $\Lambda(d; O)$ ), while in theory, it does not for the outer SISO module [18].

The mutual information values  $I$  defined in (16) will be calculated under the usual assumption of Gaussian distributed log probability estimations, and therefore, we will feed into the SISO modules values of  $\Lambda(d; I)$  and  $\Lambda(c; I)$  drawn from a known Gaussian distribution and study the corresponding output values of  $\Lambda(d; O)$  and  $\Lambda(c; O)$  for the inner and outer SISO modules, respectively [32]. For this kind of Gaussian distributed input log probabilities, the calculation of the input mutual information  $I(I)$  through (16) is quite straightforward, while the output mutual information  $I(O)$  has to be calculated through numerical integration over the histogram of the samples of the output log probability estimations  $\Lambda(d; O)$  and  $\Lambda(c; O)$ .

By combining the two  $I(O)/I(I)$  curves from the two SISO modules, we get the EXIT chart for the iterative decoder, as shown in Figs. 3–5.  $I_1$  is the input mutual information for the inner SISO module, and  $I_2$  is the corresponding output mutual information. At the same time, given that the output mutual information of the inner SISO module, after going through the deinterleaving stage, is the input mutual information for the outer SISO module,  $I_2$  is also the input mutual information for the outer SISO module, and conversely,  $I_1$  is the output mutual information for this same SISO module. This is true because the deinterleaver and the interleaver do not change the input/output distributions of the log probability estimations and their operation on the EXIT chart is a simple change in the meaning of the axis of the corresponding plot.

In this way, the iterative decoding process starts over the  $(I_1 = 0, I_2(0))$  point on the upper curve (corresponding to the inner SISO), i.e., when there is still no input mutual information. This  $I_2(0)$  value is the input value for the lower curve (corresponding to the outer SISO), and we get, at the output, a corresponding value  $I_1(I_2(0))$  from this curve, which, in turn, will be the input value for the next step at the inner SISO and

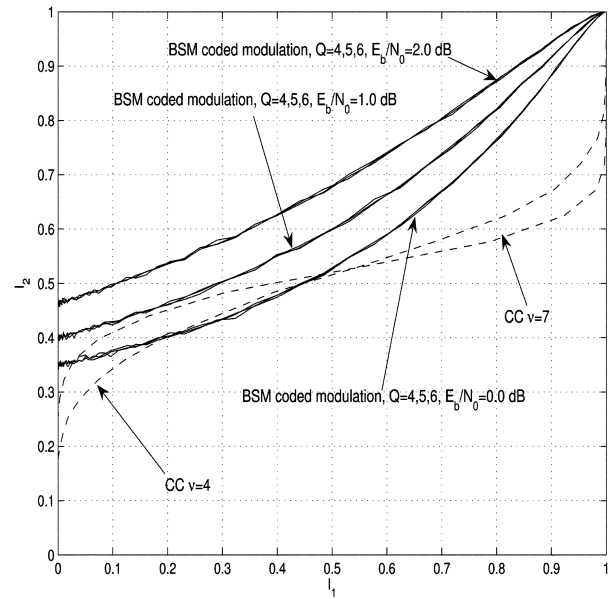


Fig. 3. EXIT chart with two different CCs and a BSM chaos-based coded modulation with  $Q = 4, 5$ , and  $6$ .

its corresponding curve. This process goes on until we reach a crossing point between the two curves where the algorithm cannot proceed further. This kind of EXIT charts assumes that the output log probability estimations from one decoding step and the input log probability estimations for the next one are uncorrelated, which is not exactly true as we iterate. Nevertheless, this situation can be approached with a good interleaver design or a large interleaver depth  $N$ [32].

In Fig. 3, where we have shown the EXIT chart for two CCs and for the BSM chaos-based coded modulator in the AWGN channel, we see clearly that this crossing point is a function of the channel distortion. If the first crossing point is the  $(1, 1)$  point, as is the case of the curves of the BSM chaos-based coded modulator for  $E_b/N_0 = 2.0$  dB with respect to the two CC curves, the algorithm truly converges, and we are in the region where the BER is dominated by the error floor and where we need just a few number of iterations to get low BER values [32]. If the final point is not the  $(1, 1)$  point, as is the case of the BSM chaos-based coded modulator curves for  $E_b/N_0 = 0.0$  dB with respect to the curves of both CCs, the algorithm gets stuck at a fixed point with a high value of BER and a high degree of uncertainty over the message sent, no matter the number of iterations performed. When the distortion in the channel is just low enough to allow the decoding process to snake through a bottleneck between the curves, we are in the waterfall region, where the algorithm starts to converge to the  $(1, 1)$  point and there is an abrupt change in the BER slope.

The CC curves of Fig. 3 have been drawn for two nonsystematic nonrecursive-rate  $R_{CC} = 1/2$  CCs of different complexities: an eight-state CC with  $\nu = 4$  and generator polynomials  $[1001 \ 1101]$  ( $d_{\text{free}} = 5$ ) and a 64-state CC with  $\nu = 7$  and generator polynomials  $[1100111 \ 1001111]$  ( $d_{\text{free}} = 8$ )[22]. Respecting the BSM chaos-based coded modulator, we see that the mutual information curves are the same for three different quantization levels, i.e.,  $Q = 4, 5$ , and  $6$  for the same  $E_b/N_0$  in the channel. This is a desirable property that hints to the relative

independence of the performance on the  $Q$  parameter. Therefore, we can just keep  $Q$  and, thus, the encoding and decoding complexity as low as possible in practice, while being able to study the system using the chaotic properties of the signal when  $Q \rightarrow \infty$ . We can thus assume that the results are steadily related to the underlying properties of the map and not to the *ad hoc* control and quantization parameter. This principle has been shown to hold, as mentioned, in the calculations of minimum Euclidean distances of systems based on 1-D discrete chaotic maps [30].

In Fig. 3, on the other hand, we can see that, for  $E_b/N_0 = 1.0$  dB, we can reach full convergence, at least theoretically, with the CC of lower complexity ( $\nu = 4$ ), while we would need additionally as much as some tenths of decibels to be able to converge with the higher complexity CC. In fact, the BSM curve for such  $E_b/N_0$  almost intersects the  $\nu = 7$  CC curve at (0.20, 0.45). This is a known property of this kind of serial concatenated system with interleavers [18], and therefore, we will prefer the CC with lower complexity but better convergence results. It is also known that the recursive inner encoder leads to a worse behavior in the first iteration and a worse BER in the low  $E_b/N_0$  region than a nonrecursive one, but once we are above the threshold, in the BER waterfall region, the performance is much better, and we get a higher coding gain.<sup>1</sup> Although, in the AWGN case, we have a threshold of at least 1.0 dB according to the figure, the BER curves of Section VI will show that, with a finite size interleaver, and as a consequence of not having exactly Gaussian distributed input log probability estimations, this threshold requires, in practice, a higher  $E_b/N_0$ .

In Fig. 4, we have plotted the EXIT chart for the CC with  $\nu = 4$  and three different cases for the BSM chaos-based coded modulation in the Rician fading channel, in the case where we have perfect CSI. When  $K = 20$  and the channel tends to be a pure AWGN one, we will almost have the same threshold as with the  $K \rightarrow \infty$  case,  $E_b/N_0 \approx 1.0$  dB. As expected, there is a gradual degradation as we tend to the Rayleigh channel, so that the threshold for  $K = 5$  is around 2.0 dB and, finally, around 3.4 dB for  $K = 0$ . As was stated with the former EXIT chart, we will see that the BER curves show an additional degradation in the  $E_b/N_0$  thresholds. In any case, we will see in Section VI that, in the fading channel with CSI, we will require up to 2.0 dB of additional signal-to-noise ratio to reach the BER waterfall region with respect to the AWGN channel results, which is a positive result that confirms that the SCCCM scheme can keep the potentially good properties of TCM-based systems in fading channels [21]. In Fig. 5, we show plots for the same situation, but without CSI. Now, the threshold is 1.6 dB higher in the Rayleigh fading case without CSI with respect to the Rayleigh fading case with CSI, and this difference tends to vanish as we approach the pure AWGN case ( $K \rightarrow \infty$ ). Again, these results will prove to be more orientative than exact.

As already mentioned, the EXIT charts shown in this paper have been developed under the usual assumptions stating that we have Gaussian distributed log probability estimations and that the interleaver depth is high enough to make the input and output log probability estimations practically uncorrelated from one iterative decoding step to the next one. In a binary turbocode

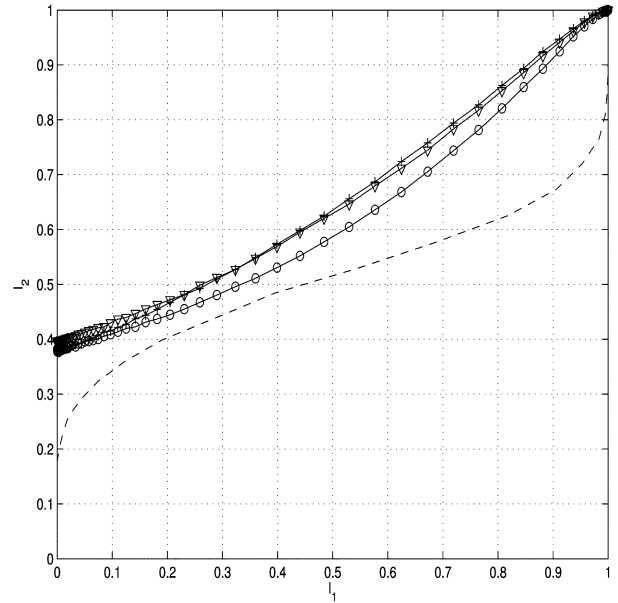


Fig. 4. EXIT chart for the (dashed line) CC with  $\nu = 4$  and a BSM chaos-based coded modulation with  $Q = 5$  for the fading + AWGN channel, in the case where perfect CSI is available at the decoder. (+)  $E_b/N_0 = 3.4$  dB and  $K = 0$ . ( $\nabla$ )  $E_b/N_0 = 2.0$  dB and  $K = 5$ . (o)  $E_b/N_0 = 1.0$  dB and  $K = 20$ .

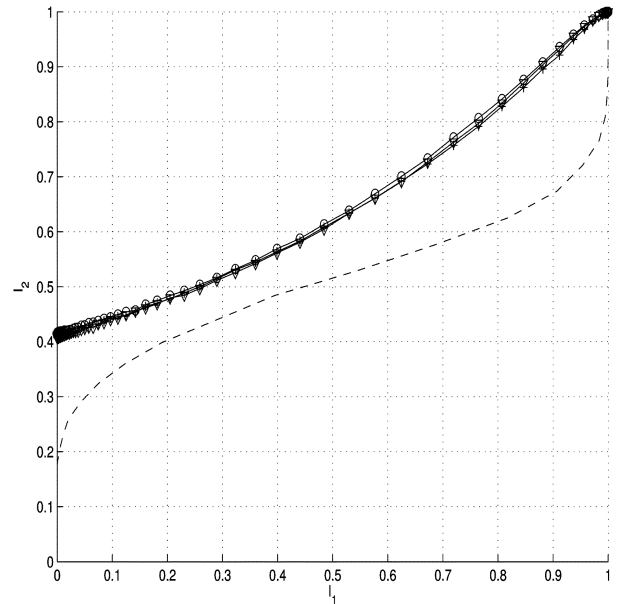


Fig. 5. EXIT chart for the (dashed line) CC with  $\nu = 4$  and a BSM chaos-based coded modulation with  $Q = 5$  for the fading + AWGN channel, in the case where there is no CSI at the decoder. (+)  $E_b/N_0 = 4.0$  dB and  $K = 0$ . ( $\nabla$ )  $E_b/N_0 = 2.2$  dB and  $K = 5$ . (o)  $E_b/N_0 = 1.4$  dB and  $K = 20$ .

with CC as constituent encoders or in usual TTCM, SCTCM, or BICM systems, the input/output log probability estimations are approximately Gaussian distributed for the AWGN channel depending on the structure of the decoder and the implementation of the related MAP algorithm. We have found that this is also the case for our SCCCM system in the AWGN channel, but it is only a loose approximation in the case of the fading channel, with or without CSI. Moreover, the Gaussian distribution assumption only becomes more or less close to the real situation as  $K \rightarrow \infty$ . Thus, we will find some mismatch between

<sup>1</sup>See [20] for the results without recursive loop.

the threshold  $E_b/N_0$  points as calculated in this section and the ones shown in the BER plots depending not only on the size and sort of the interleaver employed, which affects to the independence and uncorrelation assumption, but also on the kind of channel. Nevertheless, the threshold obtained from this EXIT chart analysis will give a good estimation of the location of the BER waterfall region when there is sufficient interleaving.

## V. ERROR-PROBABILITY ANALYSIS

To provide a bound for the bit error probability, we will make use of the developments introduced in [35]. On a first approach, they are only valid if we do not perform iterative decoding, i.e., if we perform only one decoding pass through both SISO modules. Nevertheless, they will provide us with useful bounds also for the iterative case. According to [35], we will not focus on the standard channel interface (the one whose input is  $x_n$  and whose output is  $r_n$ ). We will not try to establish the union bound with *maximum likelihood* (ML) decoding by calculating the distance spectrum of the serial concatenation of the CC and the chaos-based coded modulation. In fact, this could be a very cumbersome task because the pairwise error probability (PEP) calculated over the chaotic samples in the channel, i.e.,  $P(\mathbf{x} \rightarrow \mathbf{x}')$ , and the bit error probability are not straightforwardly related due to the nonlinear structure of the chaos-based coded modulation [13]. Even when we could make use of some simplification, the evaluation of the joint input–output weight enumerator coefficients (IOWECs), as is made in [36] for binary codes, is unfeasible in practice. Although our chaos-based coded modulation admits a description in terms of a finite-state machine and it is theoretically possible to calculate the corresponding transfer function as is done with TCM [22] or BICM [37], the method proposed here avoids this complex task.

In order to proceed without calculating the IOWEC for the chaos-based coded modulation, we will make use of the fact that the interface between  $c_n$  and  $\Lambda(c_n; \mathbf{I})$  constitutes a binary input–output symmetric (BIOS) channel when there is sufficient bit interleaving at the CC output. In this situation, we can assume that the mapping between  $\mathbf{c}$  and  $\mathbf{x}$  is independent and that the performance will depend on the binary error events  $\mathbf{c} \otimes \mathbf{c}'$  instead of on the specific values of  $\mathbf{c}$  and  $\mathbf{c}'$ . The device of the BIOS channel is normally used in the context of BICM systems [35], but we will show that it is also valid for our concatenated setup. Due to the inherent properties of the chaotic encoder, we do not need to symmetrize the channel by randomly manipulating the mapping, as is done in [19]. Therefore, we only have to focus on the finite-state machine description of the convolutional decoder and on the PEP calculated over the outputs of the deinterleaver at the receiver side (i.e., the output of the BIOS channel). Since this BIOS channel is linear, we can assume, without loss of generality, that we have sent the all-zero codeword  $\mathbf{c} = (0, \dots, 0)$ . For clarity's sake, we briefly review the method of [19], where the bit error probability is closely upper bounded by the union bound

$$P_b \leq \sum_{d=d_{\text{free}}}^{\infty} B_d \text{PEP}(d|\Theta) \quad (17)$$

where  $B_d$  is the bit enumerator of the CC for error paths leading to an output codeword with Hamming weight  $d$ ,  $\text{PEP}(d|\Theta)$  is the PEP of two codewords differing in  $d$  bits, and  $d_{\text{free}}$  is the free distance of the CC. We have introduced the variable vector  $\Theta$  which includes the parameters that define the distortion introduced by the channel and the mapping between  $c_n$  and  $x_n$ , just to clearly point out that this PEP depends on the state of the channel and on the structure of the chaos-based coded modulator. The PEP will depend on the random variable (or *equivocation*)

$$\Lambda(c; \mathbf{I}) = \Lambda = \log \left( \frac{P(c=1|\Theta)}{P(c=0|\Theta)} \right) \quad (18)$$

where we have dropped the subindex  $n$  because the sequence  $\Lambda(c_n; \mathbf{I})$  will be approximately i.i.d. under the assumption of sufficient interleaving. As shown in [35], the PEP for MAP decoding (which is the same as ML decoding in the noniterative case, since the *a priori* probabilities are the same) will be

$$\text{PEP}(d|\Theta) = \Pr \left( \sum_{i=1}^d \Lambda_i > 0 \right) \quad (19)$$

where  $\Lambda_i$  denotes  $d$  independent realizations of the random variable of (18), i.e., it is the probability of decoding a word with a Hamming weight  $d$  instead of the all-zero codeword. The tail probability of the sum of random variables of (19) can be efficiently bounded by using the cumulant transform [35]

$$\kappa(s) = \log E[e^{s\Lambda}] \quad (20)$$

where  $s \in \mathbb{R}$ .  $\kappa(s)$  is a convex function which reaches its maximum at  $\hat{s} = 1/2$ .

Taking all this into account, the bound for the PEP can be finally written as [38]

$$\text{PEP}(d|\Theta) \approx \frac{1}{2} \text{erfc} \left( \sqrt{-d\kappa(\hat{s})} \right) \leq \frac{1}{2} e^{d\kappa(\hat{s})} \quad (21)$$

where we have made use of the inequality  $\text{erfc}(\sqrt{a}) \leq e^{-a}$ . On the other side, knowing that the bit weight enumerator function (BWEF) of the CC can be expressed as

$$B(X) = \sum_{d=d_{\text{free}}}^{\infty} B_d X^d = \frac{1}{k} \frac{\partial A(X, W)}{\partial W} \Big|_{W=1} \quad (22)$$

where  $A(X, W)$  is the input–output weight enumerator function (IOWEF) and  $k = 1$  is the number of information bits per unit time,  $P_b$  can be upper bounded by

$$P_b \leq \frac{1}{2} B(X) \Big|_{X=e^{\kappa(\hat{s})}} \quad (23)$$

A tighter bound can be obtained if we make use of the inequality  $\text{erfc}(\sqrt{a+b}) \leq \text{erfc}(\sqrt{a})e^{-b}$ , where  $a > 0$  and  $b \geq 0$  [22], so that, finally

$$P_b \leq \frac{1}{2} \text{erfc} \left( \sqrt{-d_{\text{free}}\kappa(\hat{s})} \right) e^{-d_{\text{free}}\kappa(\hat{s})} B(X) \Big|_{X=e^{\kappa(\hat{s})}} \quad (24)$$

To calculate  $\kappa(\hat{s})$ , we can resort to simulating the system and storing the output samples in order to get the histogram of  $\Lambda$ , because the theoretical calculation of the pdf  $f_\Lambda(\Lambda)$  will be very difficult even for the simple AWGN channel. Moreover, it could depend, in a complex way, on the mapping between the bits and the coded modulated symbols as a function of the particular implementation of the BCJR algorithm within the SISO module. In any case, the simulations needed to get the histogram of  $\Lambda$  with enough accuracy are less time consuming than the simulations needed to give a Monte Carlo estimation of the BER, thus making it worth the while getting the described bound.

All the previous developments have been drawn for the original noniterative case. With respect to the iterative case, we can make use of the same principles and just take the histogram over  $\Lambda$  after running several decoding iterations. The channel thus described will also be a BIOS, given the structure of the SCCCM. Now, the decoding will be MAP decoding, since we are making use of the *a priori* information from the other SISO module. Following the definition of  $\Lambda$ , the PEP for this MAP decoding, assuming that the all-zero codeword has been sent, is again given by (18) and (19). Therefore, the factor  $\kappa(\hat{s})$  can again be calculated by simulation and using the corresponding histogram. Although this bound relies fundamentally on probability density estimation as is the case of the bounds based on EXIT charts [32], it will be, in general, more accurate. The reason for this is that it takes into account the specific interleaver structure and depth and it does not make any prior assumption on the kind of distribution followed by the log probability estimations. Nevertheless, due to the fact that we rely on density evolution, we will get results that are slightly better than the real ones, so that, in practice, it will appear as a lower bound.

In the examples shown along with the simulation results, we will make use of the simple  $\nu = 4$  CC of the preceding section, whose IOWEF and BWEF are, respectively, as follows:

$$A(X, W) = \frac{WX^5 - W^2X^6 + W^2X^8}{1 - 2WX - WX^3} \quad (25)$$

$$kB(X) = \frac{X^5 - 2X^6 + 2X^7 + 2X^8 - X^9 - X^{11}}{1 - 4X + 4X^2 - 2X^3 + 4X^4 + X^6} \quad (26)$$

i.e.,

$$\begin{aligned} A(X, W) &= WX^5 + W^2X^6 + 2W^3X^7 \\ &\quad + (4W^4 + 2W^2)X^8 + \dots \\ kB(X) &= X^5 + 2X^6 + 6X^7 + 20X^8 + 56X^9 + \dots \end{aligned}$$

Note that the bound of (24) for the noniterative decoding is a union bound that will converge only for high  $E_b/N_0$ , i.e., after having reached the code cutoff rate. In the case of iterative decoding, the bound will prove useful only in the waterfall BER region, but not in the error floor region. This is due to the fact that, in this last region, we cannot rely on calculations based on the evolution of the log probability estimations. This has to do partially with the structural constraints of the SISO modules (where some clipping and normalization in the log probabilities values always have to be performed in order to provide stability and avoid overflows [18]). To provide bounds for the error floor region, we would need a more involved analysis based upon a study of the ML decoding of the joint SCCCM system without

using the convenient simplification of the BIOS channel. This would be a very difficult task, but its results would be important in order to complete the error analysis of the SCCCM systems, particularly considering that the error floor BER for serially concatenated schemes cannot be reached easily by simulation [36].

## VI. SIMULATION RESULTS

For comparison, we have included the results of a rate  $R = 1/2$  SCCC consisting of the same  $\nu = 4$  outer CC as employed throughout the SCCCM examples, the same interleaver, and a rate 1 inner accumulate code. This rate 1 accumulate code has, as feedback polynomial,  $1 + D^Q$ , and, as feedforward polynomial, just 1. This structure mimics the recursive part of the BSM chaos-based coded modulator as seen in Section II, but it generates just binary outputs. The use of inner rate 1 accumulate codes in serial concatenation has shown to lead to very interesting results with a simple encoding structure [39].

In Fig. 6, we show the simulation results for the SCCCM and SCCC systems under study in the AWGN channel with different sets of parameters. For the cases with iterative decoding, we performed 20 decoding iterations both to get the BER and to get the bound, which requires calculating the histogram of the log probability estimations. First of all, as predicted through the EXIT charts, the case with  $\nu = 7$  reaches the waterfall region with an  $E_b/N_0$  threshold higher than the case with  $\nu = 4$ , for the same size and kind of interleaver and for the same quantization level in the BSM chaos-based coded modulator. We also show the BER for the same sets of parameters corresponding to the  $\nu = 4$  CC, but without decoding iteratively (i.e., only one decoding pass is performed). As expected, the decoding gain is dramatically linked to the iterative decoding of the concatenated encoded data.

Using the same analysis techniques as mentioned throughout Section V, it has been shown for the noniterative decoding of BICM [35] that the system tends to perform, when  $E_b/N_0 \rightarrow \infty$ , like the outer CC in a channel with  $\kappa(\hat{s}) \rightarrow -(d_{E_{\min}}^2/4)SNR = -(2Rd_{E_{\min}}^2/4)(E_b/N_0)$ , where  $d_{E_{\min}}^2$  is the minimum Euclidean square distance of the inner modulation. In our case, we can draw a similar bound just by taking  $d_{E_{\min}}^2 = 4/3$ , which is the minimum Euclidean square distance between all possible chaotic sequences of the BSM encoder.<sup>2</sup> Although we can only conjecture that this bound should also be valid for the noniterative decoding of our SCCCM system and a formal proof would require a complex ML study of SCCCM for high signal-to-noise ratios, we can verify through the noniterative result in Fig. 6 that it reasonably holds for this kind of coded modulation. There, we have shown the bound (24) with

$$\text{PEP}(d|\Theta) = \frac{1}{2}e^{-d\frac{2Rd_{E_{\min}}^2}{4}\frac{E_b}{N_0}} \quad (27)$$

which tends to the BER without iterative decoding for high  $E_b/N_0$ . Note that this bound is a lower bound.

The results make evident the importance of a good interleaver design, since, although the performance of the case with  $N = 400$  and  $S = 11$  without iterative decoding (not shown)

<sup>2</sup>This is the true value with  $Q \rightarrow \infty$ , but it does not differ much from the minimum Euclidean square distance for the  $Q = 5$  value of our examples [30].

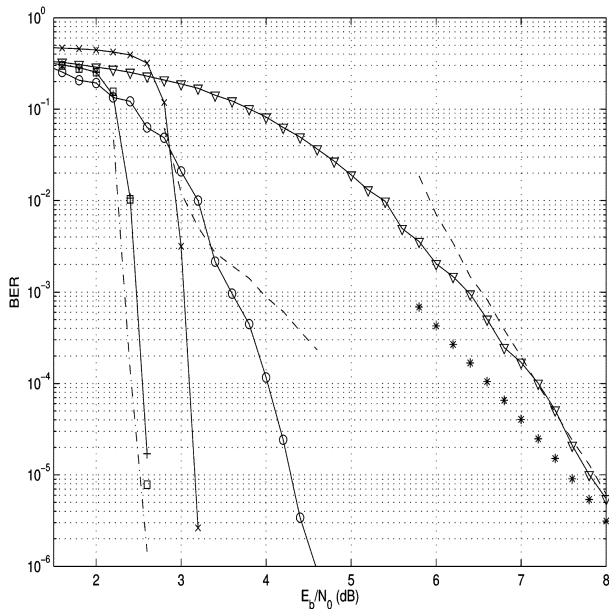


Fig. 6. BER for several cases of SCCCM in the AWGN channel. (+)  $N = 10\,000$ ,  $S = 23$ ,  $Q = 5$ , and  $\nu = 4$ . ( $\times$ ) Same parameters, but with a CC of  $\nu = 7$ . ( $\circ$ )  $N = 400$ ,  $S = 11$ ,  $Q = 5$ , and  $\nu = 4$ . ( $\nabla$ ) Same parameters as +, but without iterative decoding. (Dashed lines, from left to right) Bounds for the cases with  $\nu = 4$  and  $Q = 5$ . (\*) Bound with  $d_{E_{\min}}^2$  for the noniterative case. ( $\square$ ) Same parameters as +, but with  $Q = 4$ .

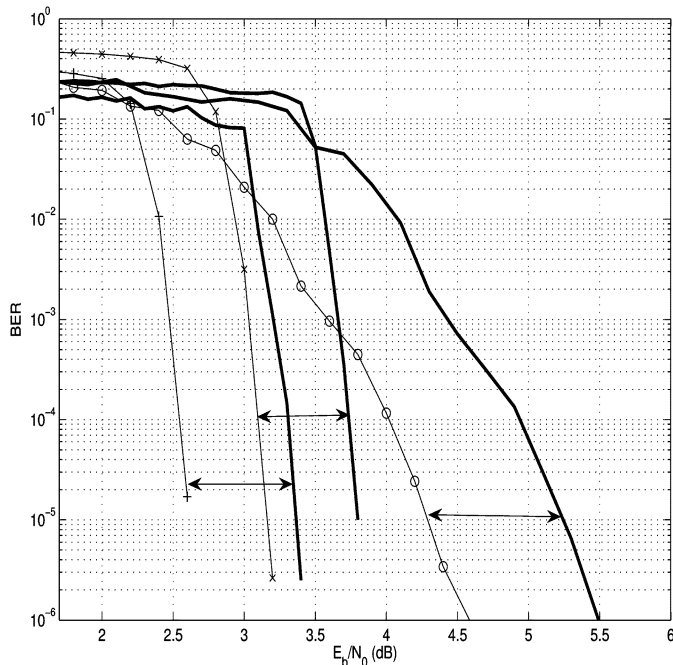


Fig. 7. BER for several cases of SCCCM and SCCC in the AWGN channel. (+) SCCCM with  $N = 10\,000$ ,  $S = 23$ ,  $Q = 5$ , and  $\nu = 4$ . ( $\times$ ) SCCCM with the same parameters, but with a CC of  $\nu = 7$ . ( $\circ$ ) SCCCM with  $N = 400$ ,  $S = 11$ ,  $Q = 5$ , and  $\nu = 4$ . The performance of the corresponding binary SCCC systems is shown by a thick line, and the difference in  $E_b/N_0$  with respect to the SCCCM counterpart is indicated by the double arrows.

is the same as the performance for the case with  $N = 10\,000$  and  $S = 23$  without iterative decoding, when decoding iteratively, there is a huge difference in the behavior of the BER. With  $N = 400$ , we have a lower BER slope, and there is no distinct waterfall region. This means that a high interleaver depth

is necessary to get good results, because a better interleaver design can provide a higher degree of uncorrelation between coded bits and channel samples and, as a consequence, more accurate *a priori* information at the beginning of each decoding pass.

We have also shown in Fig. 6 the bound of Section V for the cases with  $\nu = 4$ . As expected, the bound for the noniterative case converges as an upper union bound to the final performance when  $E_b/N_0 \rightarrow \infty$ . On the contrary, the bound for the  $N = 400$  case and iterative decoding is not very helpful. This is due to the fact that the BIOS assumption for iterative decoding only holds for sufficient interleaving, and a low value of  $N$  does not guarantee the needed symmetry. On the other hand, the bound for the  $N = 10\,000$  case and iterative decoding gives very accurate information about the location and slope of the BER at the waterfall region, although, as foreseen, appears as a lower bound instead of as an upper one. Note also that what was said about the  $E_b/N_0$  thresholds for this region as calculated through the EXIT charts is true: In the best case ( $N = 10\,000$ ), there is a difference between the expected value and the actual value of around 1.0 dB, since the EXIT chart predicted a threshold of about 1.0 dB for the CC of  $\nu = 4$  and of about 2.0 dB for the CC of  $\nu = 7$ .

On the other hand, it can also be verified in Fig. 6 that the influence of  $Q$  is small, provided that it has not a very low value,<sup>3</sup> since the BERs for  $Q = 5$  and  $Q = 4$  are virtually the same for the same set of parameters. The same holds for  $Q = 6$  and  $Q = 7$  (not shown for simplicity). In Fig. 7, we compare the performance of the SCCC system proposed with its chaos-based counterpart for the same sets of parameters shown in Fig. 6. Note that the SCCC test system is roughly equivalent to an SCCCM system with  $Q = 1$  and that it is more than 0.5 dB worse in the location of the waterfall region with respect to the chaos-based related system.

In Fig. 8, have shown the results for  $N = 10\,000$ ,  $S = 23$ , and  $\nu = 4$  for the fading channel with different degrees of impairment, both when there is CSI at the decoder and when there is no CSI. All the results have been taken after 20 iterations. Let us focus first on the SCCCM results. Again, there is a mismatch between the  $E_b/N_0$  threshold given by the simulations with respect to the expected values given by the EXIT charts. While, for the Rayleigh fading case, the expected thresholds were around 3.0 dB with CSI and 4.0 dB without CSI, the BER results place the thresholds at about 4.0 and 5.5 dB, respectively. Since the Rayleigh fading is the worst case of Rician fading, it is not surprising to see that it yields the worst results and the largest difference between the CSI and non-CSI cases. On the contrary, the results tend to the BER in the AWGN channel as  $K$  grows, both with CSI and without CSI. Even the worst case (Rayleigh without CSI) still keeps the good properties with respect to the BER slope once the waterfall region is reached, although with a loss of about 3.0 dB with respect to the pure AWGN case. For the Rayleigh fading and perfect CSI, the loss is just around 1.5 dB. These results in the fading channel are consistent with what was shown in [40] for SCCC and in [19] for BICM. We have also included the bound with iterative decoding for the Rayleigh channel with CSI, and as seen before for the AWGN

<sup>3</sup>For example, for  $Q = 1$ , we would be in the BPSK case and no chaotic dynamics would be involved. In fact, if  $Q = 1$ , we would just be in the SCCC case.

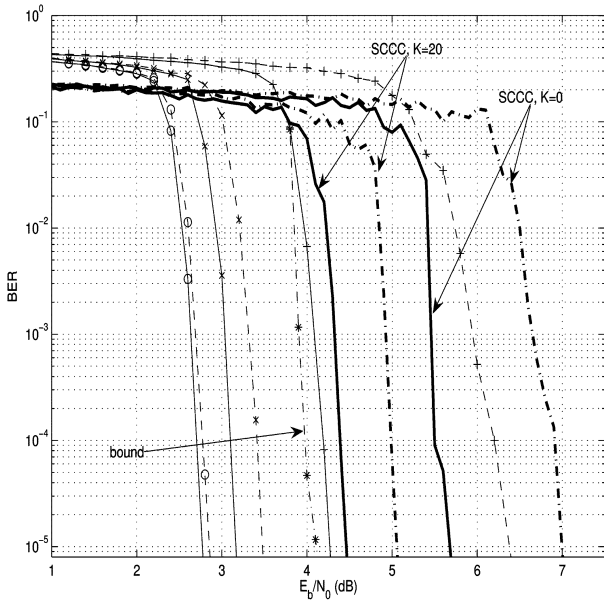


Fig. 8. BER and bounds for several cases of SCCM in the fading channel, with and without CSI. (Continuous lines) With CSI. (Dashed lines) Without CSI. In all cases,  $N = 10\,000$ ,  $S = 23$ ,  $Q = 5$ , and  $\nu = 4$ . (From left to right)  $K = 20$ ,  $K = 5$ , and  $K = 0$ . (\*) (With dashed-dotted line) Bound for  $K = 0$  and CSI. The performance of the binary SCCC is shown by a thick line for comparison.

channel, when the interleaver depth is high enough, the results approximate very accurately the location and the slope of the BER at the waterfall region.

With respect to the performance of the SCCM system, we see that the losses in the Rayleigh fading channel with CSI are some tenths of decibels worse than the results of the SCCCM system with respect to the pure AWGN channel. When  $K = 20$  and we have CSI, the comparison between the SCCCM system losses and the SCCC system losses gives advantage to the chaos-based system again for some tenths of decibels. Note that the difference of performance for SCCCM in the fading channel with  $K = 20$  between the CSI and non-CSI cases is almost negligible, while it is around 0.5 dB for the SCCC system in the same situation. On the contrary, the losses between the CSI and non-CSI cases for the same degree of fading tend to be lower for the SCCC system as we approach  $K = 0$ : 1.2 dB for SCCC against 2.1 dB for SCCCM at a BER of  $10^{-5}$  in the Rayleigh channel.

To shed light on the behavior of the iterative decoding of SCCCM, we have shown in Figs. 9 and 10 two EXIT charts where we can compare the predicted behavior with the real evolution of the mutual information. It was calculated by averaging over the log probability estimations obtained after each iteration during the simulations performed to get the BER. In this way, we get the average trajectory of the mutual information [32]. As hinted, when comparing the  $E_b/N_0$  thresholds for the waterfall region, there is a mismatch between the theoretical curves and the actual trajectory. We can see in both graphs, for the pure AWGN case and for the fading case, that only the first step corresponds with the expected value, as this is the situation when we have no feedback from the other decoder. In the rest of the steps, we always get a lower value for the mutual information with respect to the one calculated with the assumption

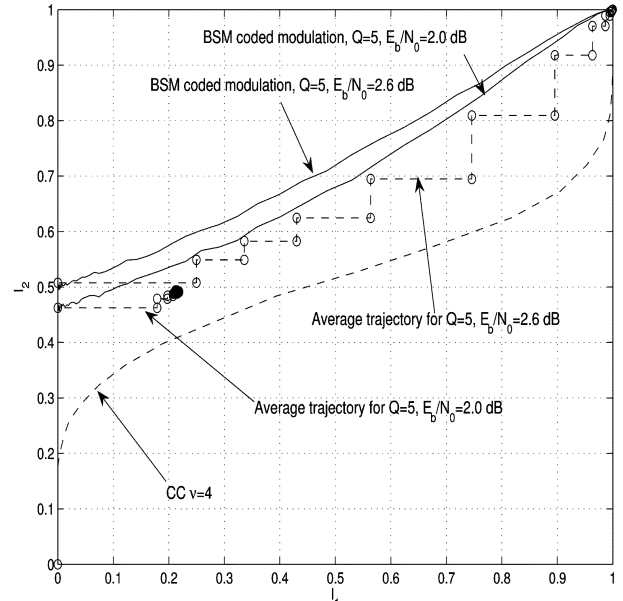


Fig. 9. EXIT chart and average trajectory of the mutual information interchange for the AWGN channel, for the case with  $Q = 5$ ,  $N = 10\,000$ , and  $S = 23$ .

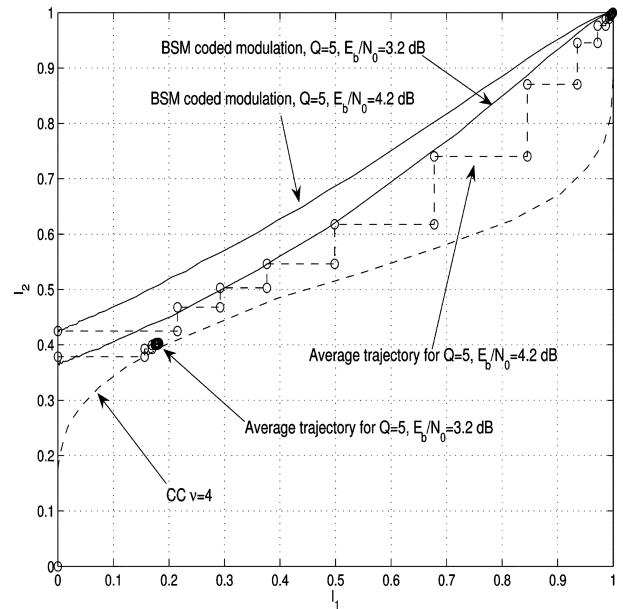


Fig. 10. EXIT chart and average trajectory of the mutual information interchange for the AWGN channel with fading, for the case with  $Q = 5$ ,  $N = 10\,000$ ,  $S = 23$ ,  $K = 0$ , and perfect CSI at the decoder.

of Gaussian distribution of the input log probability estimations. Therefore, the iterative decoding process does not achieve convergence at the first  $E_b/N_0$  value where the decoder curves do not intersect before the (1, 1) point. Apart from the Gaussian density assumption, which only holds loosely as already mentioned, there are other possible sources of mismatch, like an inappropriate definition of the mutual information or like an interleaver design not providing enough uncorrelation between channel samples and encoded bits. This last feature could be overcome by increasing the interleaver size  $N$  at the expense of a higher complexity. The loss in the  $E_b/N_0$  thresholds is the

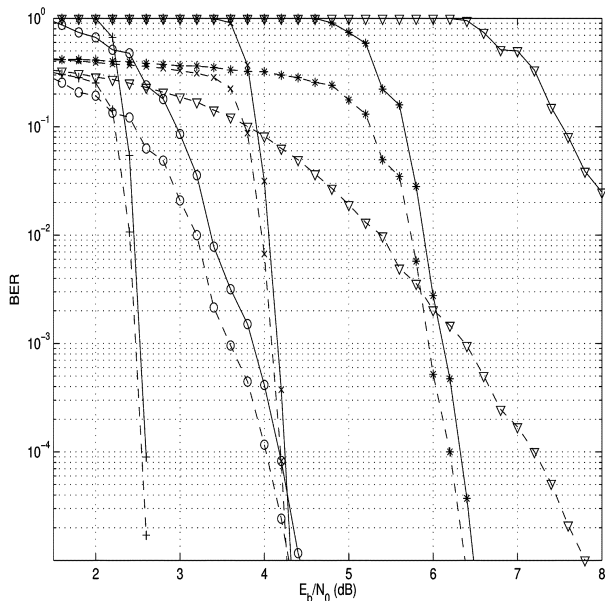


Fig. 11. FER and BER for several cases of SCCCM for the CC with  $\nu = 4$  and BSM with  $Q = 5$ . (Continuous line) FER. (Dashed line) BER. (+)  $N = 10\,000$  and  $S = 23$ . (o)  $N = 440$  and  $S = 11$ . ( $\nabla$ ) Same as +, but without iterative decoding. ( $\times$ ) Same as +, but with fading,  $K = 0$ , and CSI. (\*) Same as  $\times$ , but without CSI.

same for the pure AWGN channel and for the fading channel, and this points toward the SISO and interleaver structures as reasons for the mismatch rather than toward the differences in the channel distortion.

Finally, we have shown in Fig. 11 the frame error rate (FER) and the BER for several of the cases already commented. When there is no iterative decoding, the FER is very high and starts decreasing when the main error events are of the  $d_{\text{free}}$  kind, so that each frame on error contains only 1 bit on error and then  $BER \approx (1/k)$  FER, with  $k = R \cdot N - \nu = 4996$ . On the other hand, when decoding iteratively, this situation is highly improved, since the FER for the interleaver with  $N = 10\,000$  in the AWGN channel follows the behavior of the BER and exhibits a steep slope in the waterfall region. This means that there are less frames on error, but, as a contrast, we have found out that each frame on error contains around 1000 erroneous bits in the waterfall region, so that, now,  $BER \approx (1/5)$  FER. In the case with  $N = 400$ , the situation is the same, but now, each frame on error contains around 60 erroneous bits, and as  $k = 196$ ,  $BER \approx (1/3)$  FER. Therefore, the gain in BER and FER is made at the expense of having large bursts of errors, instead of having the dominant weight 1 error events of the noniterative case.

The situation for the fading channel is quite the same, as shown through the worst case, i.e., Rayleigh fading. In the waterfall region, the FER falls down with the same slope as the BER, and we still have the fact that each frame on error contains around 1000 erroneous bits, so that, again,  $BER \approx (1/5)$  FER, both for the CSI and non-CSI cases. Therefore, the iterative decoder behaves, at least in the waterfall region, in the same way with the independence of the kind of channel, which only seems to affect the  $E_b/N_0$  thresholds for this region. All these show that SCCCM keeps the good properties of serial concatenated systems in the fading channel (SCCC, SCTCM, and BICM), un-

coupling the channel state and the error-correcting capabilities of the code once we are above some threshold of channel distortion. It will be interesting to study what happens on the error floor region. However, since we cannot reach it easily through simulation, this would mean developing performance bounds based upon complicated ML analysis.

## VII. CONCLUSION

In this paper, we have examined the possibility of building serially concatenated coded modulations using chaos-based coded modulations as inner encoders. We have shown that the resulting system can greatly enhance the results of *a priori* bad-performing chaotic communications systems like the ones based on the BSM. We have shown that we can use the same principles and tools normally used in SCCC or BICM to design and evaluate the performance of the related concatenated systems. Although the EXIT charts drawn and the bounds proposed are not always well matched due to the assumptions made, they always give good and useful approximations. We have also shown that the chaotic properties of the modulator are a determining factor for the final performance, along with the outer binary channel encoder, with the independence of the quantization level of the underlying discrete chaotic map, at least down to a minimum value of the same.

We have verified that SCCCM can keep the good properties of SCCC, SCTCM, and BICM and exhibit the same characteristic behavior in AWGN and frequency-nonselctive flat fading channels. The resulting SCCCM systems are slightly more complex to decode than the related SCCC system because the SISO module for the chaos-based coded modulation requires more computations. Nevertheless, the BER and FER results have shown that the performance degradation in fading channels, as compared with the AWGN case, is lower as compared to the SCCC setup with similar complexity. Moreover, these chaos-based coded modulations are easy to generate and produce noise-like broadband signals suitable, among others, for multiuser environments. It is expected that a deeper conjunction of chaos theory, signal processing, and communications theory developed in the direction pointed out by the latest research works in chaos-based coded modulations will help to improve the understanding and possibilities of this new kind of concatenated systems.

## REFERENCES

- [1] S. Hayes, C. Grebogi, and E. Ott, "Communicating with chaos," *Phys. Rev. Lett.*, vol. 70, no. 20, pp. 3031–3034, May 1993.
- [2] M. Hasler and T. Schimming, "Optimal and suboptimal chaos receivers," *Proc. IEEE*, vol. 90, no. 5, pp. 733–746, May 2002.
- [3] F. C. M. Lau and C. K. Tse, *Chaos-Based Digital Communication Systems*. Berlin, Germany: Springer-Verlag, 2003.
- [4] F. J. Escribano, L. López, and M. A. F. Sanjuán, "Evaluation of channel coding and decoding algorithms using discrete chaotic maps," *Chaos*, vol. 16, no. 1, pp. 103–119, Mar. 2006.
- [5] W. M. Tam, F. C. M. Lau, and C. K. Tse, *Digital Communications With Chaos*. Oxford, U.K.: Elsevier, 2007.
- [6] S. Kozic, T. Schimming, and M. Hasler, "Controlled one- and multi-dimensional modulations using chaotic maps," *IEEE Trans. Circuits Syst. I, Reg. Papers*, vol. 53, no. 9, pp. 2048–2059, Sep. 2006.
- [7] J. Pizolato, M. Romero, and L. Goncalves-Neto, "Chaotic communication based on the particle-in-a-box electronic circuit," *IEEE Trans. Circuits Syst. I, Reg. Papers*, vol. 55, no. 4, pp. 1108–1115, May 2008.
- [8] K.-W. Wong and C.-H. Yuen, "Embedding compression in chaos-based cryptography," *IEEE Trans. Circuits Syst. II, Exp. Briefs*, vol. 55, no. 11, pp. 1193–1197, Nov. 2008.

[9] Y. Xia, C. K. Tse, and F. C. M. Lau, "Performance of differential chaos-shift-keying digital communication systems over a multipath fading channel with delay spread," *IEEE Trans. Circuits Syst. II, Exp. Briefs*, vol. 51, no. 12, pp. 680–684, Dec. 2004.

[10] G. Mazzini, R. Rovatti, and G. Setti, "Chaos-based asynchronous DS-CDMA systems and enhanced rake receivers: Measuring the improvements," *IEEE Trans. Circuits Syst. I, Reg. Papers*, vol. 48, no. 12, pp. 1445–1453, Dec. 2001.

[11] G. Mazzini, R. Rovatti, and G. Setti, "Chaos-based spreading in DS-UWB sensor networks increases available bit rate," *IEEE Trans. Circuits Syst. I, Reg. Papers*, vol. 54, no. 6, pp. 1327–1339, Jun. 2007.

[12] G. Mazzini, G. Setti, and R. Rovatti, "Chip pulse shaping in asynchronous chaos-based DS-CDMA," *IEEE Trans. Circuits Syst. I, Reg. Papers*, vol. 54, no. 10, pp. 2299–2314, Oct. 2007.

[13] F. J. Escribano, S. Kozic, L. López, M. A. F. Sanjuán, and M. Hasler, "Turbo-like structures for chaos coding and decoding," *IEEE Trans. Commun.*, vol. 57, no. 3, pp. 597–601, Mar. 2009.

[14] S. Kozic and M. Hasler, "Low-density codes based on chaotic systems for simple encoding," *IEEE Trans. Circuits Syst. I, Reg. Papers*, vol. 56, no. 2, pp. 405–415, Feb. 2009.

[15] S. Kozic and M. Hasler, "Belief propagation decoding of codes based on discretized chaotic maps," in *Proc. IEEE ISCAS*, Kos, Greece, May 2006, p. 1194.

[16] F. J. Escribano, L. López, and M. A. F. Sanjuán, "Chaos coded modulations over Rayleigh and Rician flat fading channels," *IEEE Trans. Circuits Syst. II, Exp. Briefs*, vol. 55, no. 6, pp. 581–585, Jun. 2008.

[17] F. J. Escribano, L. López, and M. A. F. Sanjuán, "Effects of intersymbol interference on chaos-based modulations," in *Proc. 2nd Int. SCS Conf.*, Hammamet, Tunisia, Nov. 2008, pp. 1–6.

[18] C. B. Schlegel and L. C. Pérez, *Trellis and Turbo Coding*. New York: Wiley, 2004.

[19] G. Caire, G. Taricco, and E. Biglieri, "Bit-interleaved coded modulation," *IEEE Trans. Inf. Theory*, vol. 44, no. 3, pp. 927–946, May 1998.

[20] F. J. Escribano, L. López, and M. A. F. Sanjuán, "Iteratively decoding chaos encoded binary signals," in *Proc. 8th IEEE ISSPA*, Sydney, Australia, Aug. 2005, vol. 1, pp. 275–278.

[21] E. Biglieri, J. Proakis, and S. Shamai, "Fading channels: Information-theoretic and communications aspects," *IEEE Trans. Inf. Theory*, vol. 44, no. 6, pp. 2619–2692, Oct. 1998.

[22] S. Lin and D. J. Costello, Jr., *Error Control Coding*. Upper Saddle River, NJ: Prentice-Hall, 2004.

[23] J. Schweizer and T. Schimming, "Symbolic dynamics for processing chaotic signals—II: Communication and coding," *IEEE Trans. Circuits Syst. I, Reg. Papers*, vol. 48, no. 11, pp. 1283–1295, Nov. 2001.

[24] R. Koetter, A. C. Singer, and M. Tüchler, "Turbo equalization," *IEEE Signal Process. Mag.*, vol. 21, no. 1, pp. 67–80, Jan. 2004.

[25] H. M. Tullberg and P. H. Siegel, "Serial concatenated trellis coded modulation with inner rate-1 accumulate code," in *Proc. GLOBECOM*, San Antonio, TX, Mar. 2001, vol. 2, pp. 936–940.

[26] F. J. Escribano, L. López, and M. A. F. Sanjuán, "Exploiting symbolic dynamics in chaos coded communications with maximum a posteriori algorithm," *Electron. Lett.*, vol. 42, no. 17, pp. 984–985, Aug. 2006.

[27] J. Hokfelt, O. Edfors, and T. Maseng, "On the theory and performance of trellis termination methods for turbo codes," *IEEE J. Sel. Areas Commun.*, vol. 19, no. 5, pp. 838–847, May 2001.

[28] E. K. Hall and S. G. Wilson, "Design and analysis of turbo codes on Rayleigh fading channels," *IEEE J. Sel. Areas Commun.*, vol. 16, no. 2, pp. 160–174, Feb. 1998.

[29] G. Xiaofeng, W. Xingang, Z. Meng, and C. H. Lai, "Chaotic digital communication by encoding initial conditions," *Chaos*, vol. 14, no. 2, pp. 358–363, Jun. 2004.

[30] S. Kozic, K. Oshima, and T. Schimming, "Minimum distance properties of coded modulations based on iterated chaotic maps," in *Proc. 11th Int. NDES Workshop*, Scuol, Switzerland, May 2003, pp. 141–144.

[31] H. Andersson, "Error-correcting codes based on chaotic dynamical systems," Ph.D. dissertation, Dept. Elect. Eng., Linköping Univ., Linköping, Sweden, 1998.

[32] S. ten Brink, "Convergence behavior of iteratively decoded parallel concatenated codes," *IEEE Trans. Commun.*, vol. 49, no. 10, pp. 1727–1737, Oct. 2001.

[33] H. Chen and A. Haimovich, "Exit charts for turbo trellis-coded modulation," *IEEE Commun. Lett.*, vol. 8, pp. 668–670, Nov. 2004.

[34] R. Otnes and M. Tüchler, "Exit chart analysis applied to adaptive turbo equalization," in *Proc. Nordic Signal Process. Symp. Board*, Hurlgruten, Norway, Oct. 2002.

[35] A. Martínez, A. Guillén i Fábregas, and G. Caire, "Error probability analysis for bit-interleaved coded modulation," *IEEE Trans. Inf. Theory*, vol. 52, no. 1, pp. 262–270, Jan. 2006.

[36] S. Benedetto, D. Divsalar, G. Montorsi, and F. Pollara, "Serial concatenation of interleaved codes: Performance analysis, design and iterative decoding," *IEEE Trans. Inf. Theory*, vol. 44, no. 3, pp. 909–926, May 1998.

[37] K. R. Narayanan and G. L. Stüber, "A serial concatenation approach to iterative demodulation and decoding," *IEEE Trans. Commun.*, vol. 47, no. 7, pp. 956–961, Jul. 1999.

[38] A. Guillén i Fábregas, A. Martínez, and G. Caire, "Error probability of bit-interleaved coded modulation using the Gaussian approximation," in *Proc. CISS*, Princeton, NJ, Mar. 2004, pp. 17–19.

[39] A. Abbasfar, D. Divsalar, and K. Yao, "Accumulate-repeat-accumulate codes," *IEEE Trans. Commun.*, vol. 55, no. 4, pp. 692–702, Apr. 2007.

[40] J. Yuan, W. Feng, and B. Vucetic, "Performance of parallel and serial concatenated codes on fading channels," *IEEE Trans. Commun.*, vol. 50, no. 10, pp. 1600–1608, Oct. 2002.



**Francisco J. Escribano** (S'07–M'08) received the B.S. degree in telecommunications engineering from the Escuela Técnica Superior de Ingenieros de Telecomunicación, Universidad Politécnica de Madrid, Madrid, Spain, and the Ph.D. degree from the Universidad Rey Juan Carlos, Móstoles, Spain.

He is currently an Associate Professor with the Departamento de Teoría de la Señal y Comunicaciones, Universidad de Alcalá de Henares, Alcalá de Henares, Spain, where he is involved in several undergraduate and master courses in telecommunications engineering. He has been a Visiting Researcher with the Politecnico di Torino, Torino, Italy, and with the Ecole Polytechnique Fédérale de Lausanne, Lausanne, Switzerland. His research activities are focused on communications systems and information theory, mainly on the topics of channel coding, modulation, and multiuser detection, and on the applications of chaos in engineering.



**Luis López** received the B.S. degrees in telecommunications engineering from the Escuela Técnica Superior de Ingenieros de Telecomunicación, Universidad Politécnica de Madrid, Madrid, Spain, and from the Ecole Nationale Supérieure des Télécommunications (Télécom Paris), Paris, France, in 1999, and the Ph.D. degree in computer science from the Universidad Rey Juan Carlos, Móstoles, Spain, in 2003.

He is currently an Associate Professor with the Universidad Rey Juan Carlos, where he coordinates/collaborates in several undergraduate and master courses in computer science and telecommunications engineering. His current research interests are concentrated on the applications of complex networks and game theory in the field of computer science in general and IP networks in particular. He has coauthored more than 50 research publications in top scientific journals and conferences.



**Miguel A. F. Sanjuán** received the B.S. degree in physics from the University of Valladolid, Valladolid, Spain, in 1981, and the Ph.D. degree in physics from the National University at a Distance, Madrid, Spain, in 1990.

He was a Visiting Research Associate with the Institute of Physical Science and Technology, University of Maryland at College Park, from July 1995 to September 1996. He was a Visiting Researcher with the University of Tokyo, Tokyo, Japan, in February 2002. Since 2002, he has been a Full Professor of Physics with the Universidad Rey Juan Carlos, Madrid, Spain, where he is the Head of the Departamento de Física and Head of the Nonlinear Dynamics, Chaos and Complex Systems Group.

Dr. Sanjuán is a Japan Society for the Promotion of Science Fellow. In 2008, he was elected as a Foreign Member of the Lithuanian Academy of Sciences.